Intervene effect on *Streptococcus suis* biofilm formation of emodin extracted from *Rheum officinale* Baill

Yang Tang
Northeast Agricultural University
Jingwen Bai
Northeast Agricultural University
Yu Yang
Northeast Agricultural University
Xuedong Bai
Northeast Agricultural University
God'spower Bello-Onaghise
Northeast Agricultural University
Yaqin Xu (xuyaqin@neau.edu.cn)
Northeast Agricultural University
Yanhua Li
Northeast Agricultural University

Research

Keywords: Rheum officinale Baill, ultrasonic-assisted extraction, emodin, Streptococcus suis, biofilm, Molecular docking, natural product

Posted Date: July 23rd, 2020

DOI: https://doi.org/10.21203/rs.3.rs-45019/v1

Abstract

Background

Streptococcus suis is a zoonotic pathogen that causes serious systemic infections in pigs and humans. It is a great threat to pig breeding and public health safety. The formation of biofilm was one of the main reasons that it's difficult to cure. Rhubarb water extract can inhibit the formation of biofilm of *Streptococcus suis*, but the main functional ingredient was not clear. And what's the potential mechanism of emodin intervene the biofilm formation? Importantly, the gene expression of *luxS* of *Streptococcus suis* was significantly decreased with emodin treatment, if there is a possibility that emodin could combine with LuxS protein which in turn inhibit the formation of biofilm?

Methods

Optimization of green ultrasonic extraction of emodin from *R. officinale* by Response Surface Methodology. The activity of antibacterial was evaluated by MIC assay. And the ability that intervene biofilm formation was evaluated through Crystal violet staining and SEM. The combination mode between emodin and LuxS protein was identified through molecular docking.

Results

The optimum extraction conditions (ethanol concentration of 80%, extraction time of 21 min, and liquid to solid ratio of 12.5:1 mL/g) were determined through the interaction analysis of different influencing factors and model verification experiment. The minimal inhibitory concentration (MIC) of RUEP against S.suis was 15.625 μg·mL-1, and sub-inhibitory concentrations of RUEP (1/2, 1/4, 1/8 and 1/16 MIC) significantly inhibited the biofilm formation of S. suis. Moreover, scanning electron microscopy analysis confirmed that RUEP can damage the layered colony community structure in biofilm and effectively intervene in the biofilm formation of *Streptococcus suis*. Through molecular docking analyzed, the inhibition of biofilm formation could be realized through the formation of hydrogen bond with residues His14 and Glu 60, π-π staking with His61Phe80 and hydrophobic interaction with Cys127.

Conclusion

Through our study, we found emodin have good antibacterial and antibiofilm formation properties and the potential mechanism of emodin intervention on biofilm formation of *Streptococcus suis* was inferred.

Background

Streptococcus suis (*S.suis*) is a zoonotic pathogen that causes serious systemic infections in pigs and humans [1]. It can cause severe diseases such as meningitis, pneumonia, septicaemia, sepsis and

arthritis even death in human [2]. And human can be infected by contacting with pigs or pork products through skin wounds or consumption of raw pork [3]. Since 1968 the first case of human infection with *S.suis* has appeared in the Denmark, growing numbers of human cases were reported in many countries. During the 1998 and 2005 Chinese epidemics, a total of 240 people were infected with *S.suis*, 53 of whom died[4]. At Thailand in 2010, the incidence proportions of the disease were 6.4/10000 persons, and the fatality rate is as high as 16.5% [5]. At Hong Kong, a great number of housewives presumably infected due to contact with (contaminated) pork product [6]. Besides, *S.suis* is predominantly an occupational hazard in North America and Europe[7, 8]. From here we see that *S.suis* and the diseases it causes do great harm to public health.

Biofilm formation is a unique life phenomenon for bacteria to adapt to the living environment. More than 1/2 all human microbial infections can be associated with biofilms, emphasizing the impact of biofilm structure on public health [9]. Most clinically isolated *S. suis* strains can form a three-dimensional layered structure (Biofilm), which is surrounded by self-secreted extracellular matrix to fight against the phagocytosis and clearance of the host and the sterilization of antibiotics [10, 11]. Biofilm formation is the main reason why *S.suis* is difficult to cure and recurrent. Biofilm helps *S.suis* evade the host's defense and resist the intervention of antibiotics. Biofilm formation was described as a process whereby bacteria adhere to the surfaces of materials (living and non-living), secrete polysaccharide matrix, fibrin, lipoprotein, etc and surround a large number of bacterial aggregate membranes [12]. The protective cover of biofilms prevents antibiotics getting access to target bacteria. In addition, the lack of oxygen supply and the accumulation of metabolites in the biofilm make the bacteria grow slowly and be insensitive to antibiotics, which are the main reasons for the bacterial resistance. The extracellular matrix of biofilm acts as a physical barrier and isolates bacteria from the body's immune system, thus deprives natural killer cells, phagocytes, specific antibodies, lysozymes, sensitized T cells and other immune effects on the bacteria [13]. At present, erythromycin, azithromycin, tylosin and aspirin are often applied to stop the biofilm formation of *S.suis*. However, the fact is that antibiotics and nonsteroidal antibacterial that can effectively kill planktonic bacteria are unable to kill bacteria in extracellular membranes of biofilms. Furthermore, drug residues in pig and human, multiple resistance [14], allergy and gastrointestinal bleeding and other problems would arise after long-term application of common antibiotics. Thus, the discovery and development of bioactive compounds from traditional Chinese medicine has become a hot spot in the field of against bacteria [15, 16].

Typically, the process of biofilms formation is mainly mediated by bacterial communication through the Quorum-sensing (QS) signaling system [17]. The QS system was responsible for the biofilm formation antibiotic resistance group behavior etc [18]. Importantly, QS system could be activated in the condition of chemical signal autoinducer-2 (AI-2) combined with the related acceptor [19]. The LuxS protein was a key enzyme in the process of AI-2 synthesis. And the LuxS/AI-2 mediated QS system play a vital role in biofilm formation of *S.suis* [20]. Research found that the gene expression of *luxS* of *S.suis* was significantly decreased with emodin treatment[21],the LuxS protein may be a target for emodin.

R. officinale, as one of the most traditional medicinal materials, has been used for thousand years. Moreover, *R. officinale* has been included in China Pharmacopoeia, British Pharmacopoeia, European Pharmacopoeia, Korean Pharmacopoeia, and Japan Pharmacopoeia due to its extensive anti-inflammatory and bacteriostatic effects [22]. Emodin (1,3,8-trihydroxy-6-methylanthraquinone) is the main bioactive component of *R. officinale*. Through many investigations, researchers have confirmed the wide spectrum pharmacological effects of emodin, including anti-cancer [23], anti-metastasis [24], reversion of multidrug resistance [25, 26], anti-inflammation [27], anti-virus [28], anti-bacteria [29, 30], and so on. Furthermore, derivatives obtained by structural modification of emodin have also been observed to have beneficial bioactive effects [31, 32]. Currently, natural emodin is mainly obtained from *Rheum palmatum* L., *Rheum tanguticum* Maxim ex Balf, and *R. officinale*. Among them, *R. officinale* is the most abundant source with the lowest price than the others. Therefore, it is vital to find an effective method for extraction of emodin from *R. officinale* with high yield to realize and expand its potential applications in the food, nutraceutical and pharmaceutical industry.

Currently, the major extraction methods for bioactive compounds are mainly the conventional ones including decoction, reflux and percolation [33]. The disadvantages of traditional extraction methods are obvious, such as time wasting, energy sapping and low yield [34]. Over the past years, ultrasound-assisted extraction (UAE) has developed rapidly and is gradually maturing. With the advantages of higher product yield, shorter working time and lower cost, UAE is gradually replacing the traditional methods. Besides, UAE is environmentally friendly while achieving high yield, which is in line with the trend of green extraction [35, 36]. More importantly, its low energy consumption and cost, satisfy the needs of industrial production of natural products.

A previous study from our laboratory observed that the water extract of *R. officinale* can intervene with the biofilm formation of *S.suis* [37]. However, it is not clear which ingredients from *R. officinale* played the major role in this process. In this study, UAE was applied to extract the active ingredient from *R. officinale*. And the optimum conditions were investigated by RSM. Besides, high performance liquid chromatograph-tandem mass spectrometry (HPLC-MS/MS) was carried out to identify the main active ingredient extracted from *R. officinale*. Finally, methods of crystal violet staining and scanning electron microscopy (SEM) were used to detect the inhibitory effect of ethanol extract of *R. officinale* on the biofilm formation of *S.suis*. The whole experiment flow is shown in Fig. 1.

Put Fig. 1 here.

Materials And Methods

Bacteria strain and cultural condition

S. suis (ATCC 700794) strain was purchased from American Type Culture Collection (ATCC) and maintained in 50% glycerin at -40 °C. The bacteria were cultured at 37 °C in

Todd Hewitt Broth (THB) medium (Summus Ltd, Harbin, Heilongjiang, China) when performing the experiments

Sample preparation and reagents

Samples of dried rhubarb (*Rheum officinale* Baill) plants were purchased from Three-trees herbal medicine market (Harbin, China). All the samples were smashed into powdery form using a disintegrator (xuman-2000y, Boou, Zhejiang, China), then filtered using a 50-mesh sieve (Beijing, China). Subsequently, the *R. officinale* powder was dried in an oven (YHG-9055A, Yaoshi instrument, Shanghai, China) at a temperature of 80 °C for 24 h and stored in a vacuum dish. Standard emodin of 98% purity was purchased from Solarbio (Beijing, China). Besides, all of other reagents used were of analytical grade. The methanol, crystal violet and glacial acetic acid were purchased from Aladdin (Shanghai, Chian).

Establishment of standard curve for emodin

First, 6.8 mg of standard emodin was added to a volumetric flask containing 50.0 mL of absolute ethanol. Aliquot of 1.0, 2.0, 3.0, 4.0 and 5.0 mL standard emodin solutions were mixed thoroughly with 1% magnesium acetate-ethanol solution in the volumetric flasks, and then these flasks were kept at room temperature for 15 min. Before measuring the absorbance of the standard emodin solutions, full wavelength scanning was carried out to determine the maximum absorption wavelength ($\lambda_{\max}$). Finally, the absorbance was measured at $\lambda_{\max}$ of 507 nm against a blank sample without emodin using a UV spectrophotometer (UV-6000PC, Shanghai Yuan Analysis Instrument, Shanghai, China). A relationship between absorbance and concentration of emodin was obtained and expressed by the following regression equation:

$$Y = 312.65X - 0.007 \quad R^2 = 0.9998$$

(1)

where Y is the absorbance of emodin solution and X (mg/mL) is the concentration of the emodin sample solution.

UAE procedure

An ultrasonic cell breaker (JY92-2D, Ningbo Scientz Technology Co. Ltd., Jiangsu, China) has been used for UAE of emodin from *R. officinale*. 0.5 g of *R. officinale* powder was poured into a beaker and a certain volume of ethanol with different concentrations was added at different liquid to solid ratios. The ultrasonic tip was submerged in the solution with a fixed depth of 2.0 cm and then UAE was conducted under ultrasonic power of 500 W for various periods of time at room temperature. The temperature of the system was maintained by adding ice on beaker surrounding. The suspension obtained was centrifuged at 8000 rpm (GL-20G-□, Shimadzu, Japan) for 15 min at room temperature. Finally, the samples were measured at 507 nm according to the method mentioned above and the contents of emodin in solutions were computed according to the standard curve obtained in 2.3.1.

Single-factor experiments of UAE

In order to explore the best conditions of UAE for emodin, three variables including ultrasonic time, ethanol concentration and liquid to solid ratio were investigated. The ultrasonic time varied from 10 to 30 min; the variation of ethanol concentration was from 50% to 90%; and the liquid to solid ratio was from 5 to 15 (mL/g), respectively. When one of the variables was investigated, the remaining variables were fixed at a certain level.

Experimental design

Based on the results obtained from the single-factor experiments, ethanol concentration (X_1), ultrasonic time (X_2) and liquid to solid ratio (X_3) were the three variables selected and

the effect of their interactions on the yield of emodin (Y) was investigated by using RSM. The three-factor-three-levels Box-Behnken design (BBD) of RSM was carried out by using Design-expert software (version 8.0), and all the independent variables that to be encoded were varied over three levels (-1, 0, 1). As a result, X_1 was varied over a range of 70%–90%. X_2 was varied from 15 to 25 min. Likewise, X_3 was changed from 10 to 15 mL/g. Besides, the codes and its representative values were shown in Table 1. The process of coding was carried out based on equation below [38]:

$$X_i = \frac{x_i - x_0}{\Delta x} (i = 1,2,3) \quad (2)$$

Put Table 1 here

where X_i and x_i represent the dimensionless and actual values of the independent variable i, x_0 is the actual value in the middle of the domain, Δx means the increment of x_i corresponding to the variation of X_i at one unit.

BBD-matrix consisted of 17 groups of experimental runs including 12 factorial points and 5 central points. Additionally, the details of the experimental conditions and the relevant experimental and predicted values of emodin yields were given in Table 2. The relationship between dependent and independent variables was expressed as a second-order polynomial equation:

$$Y = \beta_0 + \sum_{i=1}^{k} \beta_i X_i + \sum_{i=1}^{k} \beta_{ii} X_i^2 + \sum_{i \le j}^{k} \beta_{ij} X_i X_j$$

(3)

where Y is the predicted response (the yield of emodin), X_i and X_j are the coded values of the independent variables. β_0, β_i, β_{ii}, and β_{ij} represent the regression coefficients for the mean, linear, interaction and quadratic terms respectively and k is the number of independent variables (k=3 in this investigation).

All experiments were tested in triplicate and data were analyzed by Design-expert software (version 8.0). The adequacy of the mathematical model was evaluated by analysis of variance (ANOVA), the regression coefficients, coefficient of determination, and the line of best fit. On the basis of the optimum conditions predicted by RSM, additional experiments were done to compare the obtained data with the predicted value, which in turn verify the validity of the model.

Under the optimum UAE conditions, the extraction solution was collected, concentrated, lyophilized, and the crude extract was obtained. Hereafter, the crude extract was purified by using a macroporous resin and then stored at -20 °C prior to further analysis. The purified sample was termed “RUEP” and its purity (P) was calculated according to the formula: P (%) = $C_R V_R$*100/m_R, where in C_R and V_R were the concentration of emodin (mg/mL) and the volume (mL) of sample solution, respectively, and m_R was the mass of frozen sample (mg).

Put Table 2 here

Identification of emodin in RUEP by HPLC-MS/MS

HPLC-MS/MS was applied to analyze the active ingredient in RUEP. During the process of separation of sample, an ACQUITY UPLC BEH C18 column (100 mm × 2.1 mm, 1.7 mm)

was connected to a HPLC system (SCIEX ExionLC™ AD) and kept at a temperature of 40 °C. Importantly, gradient elution was carried out in this experiment. Details were as follows: 0 min, 5% solvent B; 5 min, 95% solvent B; 11 min, 95% solvent B; 12 min, 5% solvent B and 15 min, 5% solvent B. Besides, the mobile phase A and B were 0.1% formic acid and acetonitrile, respectively. The injection volume and flow rate of mobile phase were set at 5 µL and 0.4 mL/min, respectively. The detection system was mass spectrometer (TripleTOF® 5600+, SCIEX, USA) equipped with an electrospray ionization (ESI) source. Identification process was performed under positive mode and the electrospray ionization voltage was set at 5500 V. Besides, the temperature of the source was kept at 550 °C. The pressure of nebulizer gas and heater gas was 50 psi, while the curtain gas was maintained at 35 psi. In positive ESI mode, the scan range of MS was 100–1200 m/z and MS^2 were 100–1000 m/z. Nitrogen was used in each gas path with pressure of 50 psi, and the flow rate was of 10.0 L/min. ESI-MS and ESI-MS^2 were 90 V in the declustering potential. The collision energy for ESI-MS and ESI-MS^2 were 10 V and 35 V, respectively. The collision energy spread of ESI-MS^2 was 15 V. The multiple reaction monitoring mode was applied on detection. Data collection and analysis were performed by using Analyst 1.5 software.

Determination of minimal inhibitory concentration (MIC)

MIC of RUEP was determined by using the Clinical and Laboratory Standards Institute (CLSI) guidelines as referenced [39]. Briefly, overnight culture of *S.suis* was dissolved in 5.0 mL of THB medium at 37 °C and then was diluted to a final concentration of 1×10^5 CFU/mL. Subsequently, serial dilutions of the antibiotics (20 µL) were added into a 96-well microplate and then 180 µL of bacterial suspension was added. 200 µL of bacterial suspension without any antibiotics was selected as a control. After incubation at 37 °C for 24 h, the sample was taken from 96-well plate for observation. MIC was determined as the lowest concentration of antibiotics showing no visible bacterial growth and the control group was viewed as a reference

Effect of RUEP on biofilm formation

Biofilm assay was performed in line with the procedure described previously [40]. Briefly, based on the MIC procedures, the culture time was prolonged to 72 h. The medium was discarded, and then phosphate buffer saline (PBS, pH 7.2) was added into each well to wash away the floating bacteria. After pouring out PBS, 200 μL of 99% methanol was added and the mixture was incubated for 30 min to fix the biofilm. Subsequently, the methanol was poured out, and every well was dyed with 200 μL of crystal violet solution for 30 min. In the end, crystal violet dye solution was discarded and wells were washed with distilled water, and then 200 μL of glacial acetic acid (33%) was added. The optical density value of this mixed solution was measured by using a microtiter plate reader (DG5033A, Huadong, Ltd., Jiangsu, China)

Scanning electron microscopy (SEM) observation

Two pieces of sterilized frosted glass were firstly put into a 6-well microplate, and then the biofilm culture was conducted according to the method mentioned above. One well without adding RUEP was used as a control group, the other well adding RUEP was used as an experimental group. After the biofilm formation of *S.suis* on frosted glass, the culture medium was discarded and 2.5% of glutaraldehyde was added, then, the mixture was placed in a refrigerator (4 °C) for 1.5 h. At the rinsing stage, 0.1 mol/L of PBS (pH 6.8) was applied three times at an interval of 10 min each. In order to achieve the purpose of dehydration, 70%, 80%, and 90% ethanol was respectively added in experimental units for one time, and then 100% ethanol was added three times at an interval of 10 min each. Next, a mixture of tert-butyl alcohol solution and ethanol (1:1) and a pure tert-butyl alcohol solution were added respectively at an interval of 15 min. The glass was stored in a refrigerator at -20 °C, and then it was pre-frozen for 30 min and dried in a Freeze dryer (ES-2030, HITACHI, Japan) for 4 h. The glass was fixed on the sample table with conductive tape and coated the gold film with a thickness of 100–150 Å using an ion sputtering coater (E1010, HITACHI, Japan). Finally, the observation of *S.suis* biofilm was carried out under an electron microscopy (S-3400N, HITACHI, Japan).

Molecular Docking

Molecular docking was one of the main methods in Computer-Aided Drug Design. The method was widely applied on discovery of drug target and study of potential mechanism of drug action [41]. The three-dimension structure of LuxS of *S.suis* was obtained from the Protein Data Bank (https://www.rcsb.org) (PDB ID: 4XCH) [42]. The emodin structure was obtained from Pubchem (https://pubchem.ncbi.nlm.nih.gov) [43]. CDOCKER was selected for docking, which was a docking method performed based on CHARMm. Besides, semi flexible docking is adopted in the docking process, namely, all the residues of protein was fixed and the chemical compound was movable. The best conformation of compound with the lowest energy was selected for further analyzed. The binding model was analyzed and visualized by PyMoL v2.0.6. software [44].

Statistical analysis

All experiments were repeated in triplicate. Statistical analysis was carried out using SPSS 19.0. And $p < 0.05$ was considered as statistically significant.

Results

Effect of variables on extraction of emodin

The influence of different single-factors on emodin yield was investigated. At single-factors experiments, only the studied factor was varied at certain range, while other variables were fixed at certain level. The details were as follows: ethanol concentration was 70%, liquid to solid ratio was 10:1 mL/g and the ultrasonic time was 20 min. Besides, the ultrasonic power was kept at 500 W in all experiments. The result from Fig. 2A indicated that emodin yield increased gradually with time prolonged, and reached peaked at 20 min in which the yield was 2.46±0.07 mg/g. But the yield began to decrease as the time prolonged beyond 20 min. As presented in Fig. 2B, the yield was found to increase progressively with increasing ethanol concentration and the high yield of 2.44±0.18 mg/g was obtained at ethanol concentration of 80%. When ethanol concentration was above 80%, the yield began to decrease slowly. As could been seen from Fig. 2C, the yield of emodin was found to increase as liquid to solid ratio increased from 5 to 12.5:1 mL/g. And the yield of emodin reached the highest point (2.28±0.15 mg/g) when the ratio was 12.5:1

mL/g. The amount of emodin happened to decrease as liquid to solid ratio increased beyond 12.5:1 mL/g. Consequently, ultrasonic time of 20 min, ethanol concentration of 80% and liquid to solid ratio of 12.5:1 mL/g were confirmed for subsequent investigation.

Put Figure 2 here

Extraction parameter optimization by RSM and analysis

Based on the result of single-factors experiments, a total of 17 groups was designed through RSM. Three factors, including ethanol concentration, ultrasonic time, liquid to solid ratio, were investigated with pairwise interaction to analyze their effects on the yield of emodin. BBD is widely applied in experimental condition optimization, especially for three-level factors with high efficiency [45, 46]. The matrix designed by BBD and corresponding results of RSM experiments were given in Table 2. Observed from Table 2, the yields of emodin were in the range of 1.79–2.94 mg/g with the change of extraction conditions. Besides, the predicted data and observed data had a close consistence, and there was no statistically significant difference (p>0.05) between them, indicating that the model built by RSM can accurately predicted the yield of emodin. The details of the predicted ANOVA model were shown in Table 3. From the data in Table 3, a second-order polynomial equation about predicted response for emodin yield was obtained by applying regression analysis on the experimental data, which was as follows (Eq. (4)).

$$Y = 2.82 + 0.090X_2 - 0.15X_1X_2 - 0.18X_2X_3 - 0.46{X_1}^2 - 0.38{X_2}^2 - 0.38{X_3}^2 \quad (4)$$

where Y represents the yield of emodin (mg/g), and X_1, X_2, X_3 represent ethanol concentration (%), ultrasonic time (min), and liquid to solid ratio (mL/g), respectively.

Importantly, the model adequacy was verified to ensure the accuracy of the results (Fig. 3). After the evaluation of the model, response surface analysis of the results was carried out, response surface graphics and contours plots of different variables was obtained (Fig. 4).

Put Table 3、Figure 3 and 4 here

Verification of model prediction

The optimum conditions for UAE were as follows: ethanol concentration of 79.38%, ultrasonic time of 20.67 min, liquid to solid ratio of 12.46 mL/g. Under the optimized conditions, the theoretical value of emodin yield was 2.82 mg/g. Considering the operability of the experimental conditions, these conditions were amended to ethanol concentration of 80%, ultrasonic time of 21.00 min, and liquid to solid ratio of 12.5:1 mL/g, respectively. Besides, three parallel experiments were carried out under these amended conditions. The yield of emodin was 2.77±0.06 mg/g, which was agreed closely to the predicted value of 2.82 mg/g.

Identification of emodin in RUEP

After treatment with macroporous resin, RUEP with the purity of 84.47 ± 0.07% was obtained. The main active substance in RUEP was identified by comparing retention time and mass spectral data with standard based on HPLC-MS/MS analysis (Fig. 5). The compound could be identified as emodin.

Put Figure 5 here

Effect of RUEP on biofilm formation of *S.suis*

The inhibition ability of biofilm formation was evaluated by MIC assay (Fig. 6A). In Fig. 6A, a series of concentrations of emodin on effect of biofilm of *S.suis* was presented, including positive control. Comparing with control, the emodin of 1/2 MIC、1/4MIC、1/8MIC could significantly inhibit biofilm formation of *S.suis*.

Put Figure 6 here

SEM observation

The structure of biofilm of *S.suis* was observed with assistant of SEM. In total two kinds of groups, one is positive control group, one is treated with 1/2 MIC emodin. The

experimental result was shown in Fig. 6B. A thick biofilm consisting of aggregates and microcolonies of *S.suis* almost completely covered the surface of the rough glass slide. A three-dimensional biofilm with multiple layers and aggregates was formed among the communicating *S.suis* cells. However, after treatment with 1/2 MIC of RUEP (7.8125 $\mu g \cdot mL^{-1}$), the complete biofilm of *S.suis* was not existed.

Molecular docking

The molecular docking result processed by PyMOL software and presented in Fig. 7. The LuxS protein structure of S.suis was shown in Fig. 7A. The blue part was alpha helix and the purple was β-folding, while the pink represented irregular curl. As can be seen in Fig. 7B, emodin could form hydrogen bond with His14 and Glu60. Besides, π-π stacking existed between emodin and His61Phe80. Emodin has interaction with Cys127 as hydrophobic interaction. The details about combination was shown in Table 4. And the binding affinity was -5.37 kcal/mol. From Fig. 7C, emodin could inserted in the cave-like active site at the LuxS protein surface and formed ligand-protein complex. Consequently, it could be considered that emodin could be well combine with LuxS protein of *S.suis*. It's consistent with induced fit theory.

Put Figure 7 and Table 4 here

Discussion

At investigation of single-factors influence on emodin yield, the overall trend is similar: With the increase of variables, it first increases to a certain vertex and then decreases. For influence of ultrasonic time, on ultrasonic extraction of rosmarinic acid from *Orthosiphon stamineus Benth* leaves, the similar tendency was found [47]. In general, the ultrasonic wave needs time to crush the cell walls of *R. officinale* and extract the cell contents. More importantly, with time increasing, the process through which solvent enters inside the cell is promoted by cavitation and heat, and thus this enables the solvent to penetrate inside the cell and dissolve the target compound [48]. However, the extracted emodin may be degraded and its structure may be destroyed when the time is too long in the ultrasonic surrounding [49]. On effect of ethanol concentration, the effect tendency was consistent with the reports on the extraction of orientin and flavonoids [50, 51]. On one hand, dielectric constant of extraction reduces with the amount of ethanol increasing, and then solvent solubility and diffusion of target components are improved, which in turn result in the high yield of emodin [52]. On the other hand, the polarity of solvent changes with the

adjustment of ethanol concentration. When ethanol concentration was around 80%, the polarity of solvent was similar with emodin and thus maximized the solubility of emodin in solvent and resulted in a higher yield. However, when the concentration of organic solvent is too high in the extracting medium, some unfavorable situation would happen such as dehydration of cells and denaturation on of cell wall proteins, which may inhibit the diffusion of the target compounds in solvent and cause a reduction in the yield of target compounds. In addition, in the presence of small amounts of water, plant materials expand more effectively, increasing the surface area of contact between the plant substrate and the solvent [53]. Finally, the effect of liquid to solid ratio is discussed. At a very low liquid to solid ratio, the volume of the extracting solvent is so small that it is unable to completely extract the target compounds from the plant [54]. With increase in the concentration of the extraction solvent, there will be a high concentration difference between the solvent and plant materials and further lead to the release of the target compound. But as the ratio was beyond 12.5:1 mL/g, emodin yield decreased, which may be due to that the transfer of ultrasonic energy was compromised in the excessive extraction solvent. Meanwhile, the dissolved quantity of other soluble matter from plant cell would increase [55].

As could be seen from Table 3, the model had an *F*-value of 25.57 with a very low probability ($p = 0.0002$), suggesting that the model was significant. There was only a 0.01% chance that an *F*-value this large could occur due to chance. Parameters such as the determination co-efficient (R^2), adjusted determination co-efficient (R^2_{adj}) and co-efficient of variance (*C.V*%) were considered as the indices to evaluate the applicability of the model [56]. The value of R^2 was 0.9705, indicating the powerful correlation among the anticipated and experimental values. Besides, the value of R^2_{adj} was 0.9325 indicated the experimental values could be expected by using the model considerably. Furthermore, the predicted determination coefficient value (R^2_{pre}, 0.8188) was in reasonable agreement with the value of R^2_{adj}. Lower value of *C.V*% (4.78) suggested experimental values and predicted values had subtle deviations, which also indicated a high degree precision and reproducibility of the model [57]. Moreover, the adequacy of the built model to completely explain the experimental data depends on the value of lack-of-fit. The *F*-value of lack of fit was 1.64 ($p = 0.3148$), proving it was not significant compare to the pure error and good fitting degree of the regression model [58]. Besides, the coefficients of terms including X_2, X_1X_2, X_2X_3, X_1^2, X_2^2 and X_3^2 were significant for the mathematical model with *p*-value less than 0.05. By contrast, *p*-value greater than 0.05 means the model term was non-significant, such as X_1, X_3 and X_1X_3. As a result, only the terms with significant coefficient were applied for model building (shown in Eq. (4)). Moreover, the model had a maxima point for yield, namely, the predicted value, due to the quadratic coefficients of X_1^2, X_2^2 and X_3^2 were negative. A full analysis was carried out on *F*-values of the items in the regression model, the order of significance for variable that influenced the yield of emodin was: ultrasonic time (X_2) > ethanol concentration (X_1) > liquid to solid ratio (X_3).

The model adequacy was verified by the kinds of diagnostic plots such as predicted versus actual, normal % probability, and internally studentized residuals, which were vital for checking the accuracy and reliability of the model. The plot of normal % probability was shown in Fig. 3A. As observed, the

distribution was closed to the straight line, meaning that there was no deviation of the variance and normal distribution was observed. From analysis in Fig. 3B and Fig. 3C (the plot of internally studentized residuals), all data was in a reasonable range. Besides, as could been seen from Fig. 3D, the data was close to the straight line, proving the predicted value from the model was adequate and had a high correlation with the experimental data. Consequently, the model built by RSM was reliable for the estimation of UAE for emodin from *R. officinale*.

To investigate the interaction of these three test variables on the yield of emodin, response surface was plotted by varying two of the test variables while keeping the third factor fixed [59]. The steeper the response surface slope is and the closer the contour is to the ellipse, the more sensitive the response value is to the variety of factors [60]. The response surface result can be visualized by the two contours plots and the three-dimensional (3D) plots. The effect of the interaction between ethanol concentration (X_1) and ultrasonic time (X_2) on the yield of emodin was shown in Fig. 4A and Fig. 4D while the liquid to solid ratio (X_3) was fixed at 12.5:1 mg/L. It could be found that with increasing ethanol concentration from 70–80% and ultrasonic time from 15 to 20 min, there was a concomitant increase in the yield of emodin, while it was observed that the yield gradually decreased when these two test variables increased further. And their interaction had obvious impact on the yield because of the contours plot tended to the ellipse, which was agree with the significance analysis result of X_1X_2 from Table 3. Besides, the ultrasonic time had a significant effect on the yield due to the steep slope. Figure 4B and Fig. 4F represented the effect of ethanol concentration (X_1) and liquid to solid ratio (X_3) on the yield of emodin when ultrasonic time (X_2) was fixed at 20 min. The optimum yield of emodin was obtained when ethanol concentration and liquid to solid ratio were extremely close to center point, in which ethanol concentration was 80% and liquid to solid ratio was 12.5:1 mL/g. The contours plot was close to circle confirmed their interaction was not significant. As ethanol concentration (X_1) was fixed at 80%, the three-dimension plot and contours of interaction between ultrasonic time (X_2) and liquid to solid ratio (X_3) was presented in Fig. 4C and Fig. 4G. A similar change in emodin yield was observed with these two variables. The maximum yield of emodin was obtained when ultrasonic time and liquid to solid ratio were approximate 20 min and 12.5:1 mg/L, respectively. From Table 3, the interaction of X_2X_3 on yield was significant and with the existence of ellipse contours plot, indicating a strong interaction existed between ultrasonic time and liquid to solid ratio. This showed the interaction between these two variables can affect the yield of emodin dramatically. However, the influence of ultrasonic time was a little higher than liquid to solid ratio because of its steeper slopes.

Through comparing the experiment result with the predicted, proving the accuracy and effectiveness of the model. Moreover, the yield of emodin was improved than other extraction methods. Zhou's *et al* obtained the emodin yield of 2.53 ± 0.09 mg/g with assistance of microwave [61]. By using ultrasonic nebulization extraction method, researchers obtained the emodin yield of 2.04 mg/g [62]. Besides, Wu's *et al* extracted emodin from *Rheum palmatum* L, the yield of 2.21 ± 0.02 mg/g under optimum ultrasonic-assisted conditions [63]. Consequently, it could be considered that this optimum condition could extract emodin from *R. officinale* effectively.

In the process of identification, as could be seen from Fig. 5A, emodin standard was eluted at 5.053 min, with a $[M + H]^+$ at *m/z* 269.0460. Next, the molecular ion with *m/z* 269.0460 was selected as parent ion to perform a secondary scan, and the secondary mass spectrum of emodin was obtained in Fig. 5B. It mainly produced MS^2 fragment ion at *m/z* 225.0572 and *m/z* 241.0505. Under the same condition, the elution time of the constituent in RUEP was 5.051 min, the molecular cation from this active ingredient was detected at *m/z* 269.0458 (Fig. 5C). This result was consistent with Chen *et al*' s report [64]. Besides, it mainly produced MS^2 fragment ion at *m/z* 225.0569 and *m/z* 241.0503 through the secondary scan (Fig. 3D). Through analysis the primary and secondary mass spectra, the data from emodin standard and the main active ingredient in RUEP was basically same. Importantly, the application of secondary mass spectrometry ensured the accuracy of the results. Therefore, the main active ingredient in RUEP was identified as emodin.

Through analyzed molecular docking result, it was indicating that the emodin could combine with the LuxS protein through molecular docking. From analyzed the force between the ligand and residues, the shape of hydrophobic interaction would discharge the water molecules in the binding pocket, increasing the entropy of the system. Binding affinity of emodin to Luxs Protein was increased due to water molecules in hydrophobic environment were released. Besides, the formation of hydrogen bond leads their bond stronger. Among the above residues, His61 and Cys127 was highly conserved residues for binding in LuxS protein no matter in *S.suis* or other species, including *Enterococcus facecium*, *H. pylori*, *Vibrio cholerae*, *Vibrio harveyi*, *Escherischia coli*, *Salmonella enterica*, *Neisseria meningitidis*, *Actinobacillus pleuropneumoniae* etc [65]. In addition, Phe80 was an important substrate binding residue in *S.suis* LuxS protein that differ from other species. It's responsible for the enzymatic activity, the production of AI-2 and the ability of biofilm formation [66]. Consequently, it could be considered that emodin could be well combine with LuxS protein of *S.suis*. It's consistent with induced fit theory. We speculated the emodin would combine with LuxS protein at the active site, changing the conformation, influencing the function of the protein. When the ligand-protein complex formed, would decrease the production of AI-2 and inhibited the ability of biofilm formation. However, this is one of potential mechanism that emodin intervene the biofilm formation of *S.suis*, further exploration about the intervene mechanism needs to carried out.

Conclusion

In this study, ultrasonic-assisted extraction of emodin from *R. officinale* was optimized using RSM. The yield of emodin was 2.77 ± 0.06 mg/g under the optimum conditions, which was agreed closely to the predicted value of 2.82 mg/g. Ultrasonic time significantly influenced the yield of emodin, followed by ethanol concentration and liquid to solid ratio. The main active ingredient in RUEP extracted from *R. officinale* was identified as emodin by HPLC-MS/MS. Moreover, RUEP exhibited potent antibacterial property and inhibitory ability on biofilm formation of *S.suis*. The inhibition of biofilm formation could be realized through the formation of hydrogen bond with residues His14 and Glu60, π-π stacking with

residues His61Phe80 and hydrophobic interaction with residue Cys127. Therefore, RUEP from *R. officinale* may have potential value in the preparation of veterinary drugs and feed additives.

Abbreviations

S.suis: *Streptococcus suis*; *R. officinale*: *Rheum officinale* Baill; UAE: ultrasound-assisted extraction; SEM: scanning electron microscopy; HPLC-MS/MS: high performance liquid chromatograph-tandem mass spectrometry; QS system: Quorum-sensing (QS) signaling system; AI-2: chemical signal autoinducer-2; MIC: minimum inhibitory concentration; THB: Todd Hewitt Broth medium; BBD: Box-Behnken design; RSM: response surface methodology; CLSI: the Clinical and Laboratory Standards Institute.

Declarations

Acknowledgements

We are very grateful to teacher Li Dalong, College of Arts and science, Northeast Agricultural University, for his help and guidance in identification.

Authors' contributions

Jingwen Bai, Yaqin Xu: Conceptualization, Methodology. Yang Tang: Data curation, Writing-Original draft preparation. Yang Tang, XueDong Bai, Yanhua Li: Visualization, Investigation., Yanhua Li, Yaqin Xu: Supervision. God'spower Bello-Onaghise: Software, Validation.: Yaqin Xu, Yu Yang: Writing- Reviewing and Editing.

Funding

This work was financially supported by National Natural Science Foundation of China (NO. 31600276), Natural Science Foundation of Heilongjiang Province of China (NO. C2018013), Postdoctoral Scientific Research Start-up Fund Project of Heilongjiang Province of China (LBH-Q19010, LBH-Q17030).

Availability of data and materials

The data used to support this search are available from the first author upon request.

Ethics approval and consent to participate

No applicable

Consent for publication

Not applicable.

Competing interests

The authors declare that there are no conflicts of interest.

References

1. Wertheim HFL, Nihia HDT, Taylor W, Schultsz C. *Streptococcus suis*: An Emerging Human Pathogen. Clin Infect Dis. 2009;28:617–25.
2. Ma E, Chung PH, So T, Wong L, Choi KM, Cheung DT, Kam KM, Chuang SK, Tsang T. *Streptococcus suis* infection in Hong Kong: an emerging infectious disease? Epidemiol. Infect. 2008;136:1691–7.
3. Liu ZJ, Zheng H, Gottschalk M, Bai XM, Lan RT, Ji SB, Liu HC, Xu JG. Development of Multiplex PCR Assays for the Identification of the 33 Serotypes of *Streptococcus suis*. PLoS One. 2013;8.
4. Lun ZR, Wang QP, Chen XG, Li AX, Zhu XQ. *Streptococcus suis*: an emerging zoonotic pathogen. Lancet Infect Dis. 2007;7:201–9.
5. Takeuchi D, Kerdsin A, Akeda Y, Chiranairadul P, Loetthong P, Tanburawong N, Areeratana P, Puangmail P, Khamisara K, Pinyo W. Impact of a Food Safety Campaign on *Streptococcus suis* Infection in Humans in Thailand. Am J Trop Med Hyg. 2017;96:1370–7.
6. Ip M, Fung KSC, Chi F, Chau SSL, Wong BWH, Lui S, Hui M, Lai EWM, Chan PKS. *Streptococcus suis* in Hong Kong. Diagn. Microbiol Infect Dis. 2007;57:15–20.
7. Huong VTL, Ha N, Huy NT, Horby P, Nghia HDT, THiem VD, Zhu XT, Hoa NT, Hien TT, Zamora J. Epidemiology, clinical manifestations, and outcomes of *Streptococcus suis* infection in humans. Emerg Infect Dis. 2014;20:1105–14.
8. Schultsz C, Jansen E, Keikzer W, Rothkamp P, Duim B, Wagenaar JA, van der Ende A. Differences in the population structure of invasive *Streptococcus suis* strains isolated from pigs and from humans in The Netherlands. PLoS One. 2012;7.
9. Seneviratne CJ, Wang Y, Jin L, Wong SS, Herath TD, Samaranayake LP. Unraveling the resistance of microbial biofilms: has proteomics been helpful? Proteomics. 2012;12:651–65.
10. Arciola CR, Campoccia D, Montanaro L. Implant infections: adhesion, biofilm formation and immune evasion. Nat Rev Microbiol. 2018;16:397–409.
11. Ciofu O, Tolker-Nielsen T. Tolerance and Resistance of Pseudomonas aeruginosa Biofilms to Antimicrobial Agents-How P. aeruginosa Can Escape Antibiotics. Front. Microbiol. 2019;10.
12. Bai J, Yang Y, Wang S, Gao L, Chen J, Ren Y, Ding W, Muhammad I, Li Y. *Syringa oblata* Lindl. Aqueous extract is a potential biofilm inhibitor in *S. suis*. Front. Pharmacol. 2017;8:26.
13. Bonifait L, Grignon L, Grenier D. Fibrinogen induces biofilm formation by *Streptococcus suis* and enhances its antibiotic resistance. Appl Environ Microbiol. 2008;74:4969–72.
14. Boolchandani M, 'Souza D, Dantas AW. G. Sequencing-based methods and resources to study antimicrobial resistance. Nat Rev Genet. 2019;20:356–70.
15. Bai JW, Chen XR, Tang Y, Cui WQ, Li DL, God 'spower BO, Yang Y. Study on microwave assisted extraction of chrysophanol and its intervention in biofilm formation of *Streptococcus suis*. RSC Adv. 2019;9:28996–9004.

16. Zhao M, Bai J, Bu X, Tang Y, Han W, Li D, Wang L, Yang Y, Xu Y. Microwave-assisted aqueous two-phase extraction of phenolic compounds from Ribes nigrum L. and its antibacterial effect on foodborne pathogens, Food Control. 2020.
17. Kumar JS, Umesha S, Prasad KS, Niranjana P. Detection of quorum sensing molecules and biofilm formation in Ralstonia solanacearum. Curr Microbiol. 2016;72:297–305.
18. Xiao X, Wu ZC, Chou KC. A multi-label classifier for predicting the subcellular localization of gram-negative bacterial proteins with both single and multiple sites. PloS one. 2011;6.
19. Wang Y, Wang YX, Sun LY, Grenier D, Yi L. The LuxS/AI-2 system of Streptococcus suis. Appl Microbiol Biotechnol. 2018;102:7231–328.
20. Wang Y, Liu BB, Grenier D, Yi L. Regulatory mechanisms of LuxS/AI-2 System and bacterial resistance. Antimicrob. Agents Chemother. 2019;63.
21. Yang YB, Wang S, Wang C, Huang QY, Bai JW, Chen JQ, Chen XY, Li YH. Emodin affects biofilm formation and expression of virulence factors in Streptococcus suis ATCC700794. Arch Microbiol. 2015;197:1173–80.
22. Chen M, Nan TG, Xin J, Cui L, Zhang B, Wang X, Wang BM. Development of an Enzyme-Linked Immunosorbent Assay Method for the Detection of Rhein in *Rheum officinale*. Int. J. Anal. Chem. 2020.
23. Huang Q, Lu G, Shen HM, Chung MC, Ong CN. Anti-cancer properties of anthraquinones from rhubarb. Med Res Rev. 2007;27:609–30.
24. Jia XM, Iwanowycz S, Wang J, Saaoud F, Yu F, Wang Y, Hu J, Chatterjee S, Wang Q, Fan D. Emodin attenuates systemic and liver inflammation in hyperlipidemic mice administrated with lipopolysaccharides. Exp Biol Med. 2014;239:1025–35.
25. Zhang W, Chen H, Liu DL, Li H, Luo J, Zhang JH, Li Y, Chen KJ, Tong HF, Lin SZ. Emodin sensitizes the gemcitabine-resistant cell line Bxpc-3/Gem to gemcitabine via downregulation of NF-κB and its regulated targets. Int J Oncol. 2013;42:1189–96.
26. Huang L, Wang XB, Yu QM, Luo QY, Zhang ZZ. Synergistic cancer growth-inhibitory effect of emodin and low-dose cisplatin on gastric cancer cells *in vitro*. Trop J Pharm Res. 2015;14:1427–34.
27. Yao WY, Zhou YF, Qian AH, Zhang YP, Qiao MM, Zhai ZK, Yuan YZ, Yang SL. Emodin has a protective effect in cases of severe acute pancreatitis via inhibition of nuclear factor–κB activation resulting in antioxidation. Mol Med Rep. 2015;11:1416–20.
28. Ho TY, Wu SL, Chen JC, Li CC, Hsiang CY. Emodin blocks the SARS coronavirus spike protein and angiotensin-converting enzyme 2 interaction. Antiviral Res. 2007;74:92–101.
29. Dey D, Ray R, Hazra B. Antitubercular and antibacterial activity of quinonoid natural products against multi-drug resistant clinical isolates. Phytother Res. 2014;28:1014–21.
30. Cao F, Peng W, Li X, Liu M, Li B, Qin R, Jiang W, Cen Y, Pan X, Yan Z, Xiao K, Zhou H. Emodin is identified as the active component of ether extracts from *Rhizoma Polygoni Cuspidati*, for anti-MRSA activity. Can J Physiol Pharmacol. 2015;93:485–93.

31. Duan FX, Xin G, Niu H, Huang W. Chlorinated emodin as a natural antibacterial agent against drug-resistant bacteria through dual influence on bacterial cell membranes and DNA. Sci Rep. 2017;7:1–10.
32. Wen C, Zhang J, Zhang H, Dzah CS, Zandile M, Duan Y, Ma H, Luo X. Advances in ultrasound assisted extraction of bioactive compounds from cash crops–A review. Ultrason Sonochem. 2018;48:538–49.
33. Zhang LF, Liu ZL. Optimization and comparison of ultrasound/microwave assisted extraction (UMAE) and ultrasonic assisted extraction (UAE) of lycopene from tomatoes. Ultrason Sonochem. 2008;15:731–7.
34. Rombaut N, Tixier AS, Bily A, Chemat F. Green extraction processes of natural products as tools for biorefinery. Biofuels Bioprod Biorefining. 2014;8:530–44.
35. Bubalo MC, Curko N, Tomasevic M, Ganic KK, Redovnikovic IR. Green extraction of grape skin phenolics by using deep eutectic solvents. Food Chem. 2016;200:159–66.
36. Gottschalk M, Mariela S, Xu J. *Streptococcus suis* infections in humans: the Chinese experience and the situation in North America. Anim Health Res Rev. 2007;8:29–45.
37. Ding WY, Li YH, Lian H, Ai XY, Zhao YL, Yang YB, Han Q, Liu X, Chen XY, He ZG. Sub-minimum inhibitory concentrations of rhubarb water extracts inhibit *Streptococcus suis* biofilm formation. Front Pharmacol. 2017;8:425.
38. Ameer K, Chun BS, Kwon JH. Optimization of supercritical fluid extraction of steviol glycosides and total phenolic content from, *Stevia rebaudiana*, (Bertoni) leaves using response surface methodology and artificial neural network modeling. Ind. Crop. Prod. 2017;109:672–685.
39. Fothergill AW. Antifungal susceptibility testing: Clinical Laboratory and Standards Institute (CLSI) methods. In: Hall G, editors Interactions of yeasts, moulds, and antifungal agents. Humana Press. 2012.
40. Zhou YH, Xu CG, Yang YB, Xing XX, Liu X, Qu QW, Ding WY, Bello-Onaghise G, Li YH. Histidine metabolism and IGPD play a key role in cefquinome inhibiting biofilm formation of *Staphylococcus xylosus*. Front Microbiol. 2018;9:665.
41. Sliwoski G, Kothiwale S, Meiler J, Lowe EW. Computational Methods in Drug Discovery. Pharmacol Rev. 2014;66:334–95.
42. Berman HM, Westbrook J, Feng Z, Gilliland G, Bhat TN, Weissig H, Shidyalov IN, Bourne PE. The Protein Data Bank. Nucleic Acids Res. 2000;28:235–42.
43. Kim S, Chen J, Cheng T, Gindulyte A, He J, He S, Li Q, Shoemaker BA, Thiessen PA, Yu B, Zaslavsky L, Zhang J, Bolton EE. PubChem 2019 update: improved access to chemical data. Nucleic Acids Res. 2019;47:D1102–9.
44. Lill MA, Danielson ML. Computer-aided drug design platform using PyMOL. J Comput-Aided Mol Des. 2011;25:13–9.
45. Londhe V, Shirsat R. Formulation and characterization of fast-dissolving sublingual film of iloperidone using Box–Behnken design for enhancement of oral bioavailability. AAPS PharmSciTech.

2018;19:1392–400.

46. Tak JW, Gupta B, Thapa RK, Woo KB, Kim SY, Go TG, Choi Y, Choi JY, Jeong JH, Choi HG. Preparation and optimization of immediate release/sustained release bilayered tablets of loxoprofen using Box–Behnken design. AAPS PharmSciTech. 2017;18:1125–34.
47. Suhaimi SH, Hasham R, Hafiz idris MK, Mohd Ariffin NH, Abdul Majid FA. Optimization of ultrasound-assisted extraction conditions followed by solid phase extraction fractionation from *Orthosiphon stamineus Benth* (Lamiace) leaves for antiproliferative effect on prostate cancer cells. Molecules. 2019:24.
48. Balachandran S, Kentish SE, Mawson R, Ashokkumar M. Ultrasonic enhancement of the supercritical extraction from ginger. Ultrason Sonochem. 2006;13:471–9.
49. Hemwimol S, Pavasant P, Shotipruk A. Ultrasound-assisted extraction of anthraquinones from roots of *Morinda citrifolia*. Ultrason Sonochem. 2006;13:543–8.
50. Chen F, Zhang Q, Liu J, Gu H, Yang L. An efficient approach for the extraction of orientin and vitexin from *Trollius chinensis* flowers using ultrasonic circulating technique. Ultrason Sonochem. 2017;37:267–78.
51. Yang RF, Geng LL, Lu HQ, Fan XD. Ultrasound-synergized electrostatic field extraction of total flavonoids from *Hemerocallis citrina baroni*. Ultrason Sonochem. 2017;34:71–579.
52. Garcia-Castello EM, Rodriguez-Lopez AD, Mayor L, Ballesteros R, Conidi C, Cassano A. Optimization of conventional and ultrasound assisted extraction of flavonoids from grapefruit (*Citrus paradisi* L.) solid wastes. LWT-Food Sci Technol. 2015;64:1114–22.
53. Hemwimon S, Pavasant P, Shotipruk A. Microwave-assisted extraction of antioxidative anthraquinones from roots of *Morinda citrifolia*. Sep Purif Technol. 2007;54:44–50.
54. Chen FL, Du XQ, Zu YG, Yang L, Wang F. Microwave-assisted method for distillation and dual extraction in obtaining essential oil, proanthocyanidins and polysaccharides by one-pot process from *Cinnamomi Cortex*. Sep Purif Technol. 2016;164:1–11.
55. Maran JP, Mekala V, Manikandan S. Modeling and optimization of ultrasound-assisted extraction of polysaccharide from *Cucurbita moschata*. *Carbohydr* Polym. 2013;92:2018–26.
56. Maran JP, Sivakumar V, Thirugnanasambandham K, Sridhar R. Extraction of natural anthocyanin and colors from pulp of jamun fruit. J Food Sci Technol-Mysore. 2015;52:3617–26.
57. Senrayan J, Venkatachalam S. Optimization of ultrasound-assisted solvent extraction (UASE) based on oil yield, antioxidant activity and evaluation of fatty acid composition and thermal stability of *Coriandrum sativum L.* seed oil. Food Sci Biotechnol. 2019;28:377–86.
58. Martínez-Patiño JC, Gullon B, Romero I, Ruiz E, Brncic M, Zlabur JS, Castro E. Optimization of ultrasound-assisted extraction of biomass from olive trees using response surface methodology. Ultrason Sonochem. 2019;51:487–95.
59. Ai CL, Zhou DD, Wang Q, Shao XW, Lei YJ. Optimization of operating parameters for photocatalytic degradation of tetracycline using In2S3 under natural solar radiation. Sol Energy. 2015;113:34–42.

60. Gupta BS, Ako JE. Application of guar gum as a flocculant aid in food processing and potable water treatment. Eur Food Res Technol. 2005;221:746–51.
61. Lu CX, Wang HX, Lv WP, Ma CY, Xu P, Zhu J, Xie J, Liu B, Zhou QL. Ionic Liquid-Based Ultrasonic/Microwave-Assisted Extraction Combined with UPLC for the Determination of Anthraquinones in Rhubarb. Chromatographia. 2011;74:139–44.
62. Wang L, Dan L, Bao CL, You JY, Wang ZM, Shi YH, Zhang HQ. Ultrasonic extraction and separation of anthraquinones from *Rheum palmatum* L. Ultrason. Sonochem. 2008;15:738–46.
63. Wu YC, Wu P, Li YB, Liu TC, Zhang L, Zhou YH. Natural deep eutectic solvents as new green solvents to extract anthraquinones from *Rheum palmatum* L. RSC Adv. 2018;8:15069–77.
64. Zhao Y, Xie H, Zhao M, Li H, Chen X, Cai Z, Song H. Core-shell hollow spheres of type C@ MoS 2 for use in surface-assisted laser desorption/ionization time of flight mass spectrometry of small molecules. Microchim Acta. 2019;186:830.
65. Galante J, Ho AC, Tingey S, Charalambous BM. Quorum sensing and biofilms in the pathogen, Streptococcus pneumoniae. Curr Pharm Des. 2015;21:25–30.
66. Wang Y, Yi L, Wang SH, Fan HJ, Ding C, Mao X, Lu CP. Crystal Structure and Identification of Two Key Amino Acids Involved in AI-2 Production and Biofilm Formation in *Streptococcus suis* LuxS. PLoS One. 2015;10:e0138826.

Tables

Table 1 Design factor and horizontal coding of response surface methodology

Coded symbol	Independent variable	Units	Levels		
			1	0	-1
X_1	Ethanol concentration	%	70	80	90
X_2	Ultrasonic time	min	15	20	25
X_3	Liquid to solid ratio	mL/g	10.0:1	12.5:1	15.0:1

Table 2 The experimental design and results for response surface methodology

Run	Variable levels			Yield of emodin (mg/g)	
	X_1(%)	X_2 (min)	X_3 (mL/g)	Observed	Predicted
1	0(80)	0(20)	0(12.5)	2.85±0.03	2.82
2	0(80)	-1(25)	1(10)	2.17±0.06	2.17
3	-1(90)	1(15)	0(12.5)	1.94±0.02	1.87
4	1(70)	0(20)	1(10)	2.34±0.08	2.26
5	-1(90)	0(20)	-1(15)	1.97±0.11	1.99
6	1(70)	1(15)	0(12.5)	2.94±0.04	2.82
7	1(70)	-1(25)	0(12.5)	2.87±0.10	2.82
8	0(80)	0(20)	0(12.5)	1.83±0.07	1.89
9	0(80)	0(20)	0(12.5)	1.91±0.09	1.98
10	0(80)	1(15)	1(10)	1.92±0.06	2.00
11	0(80)	0(20)	0(15)	1.97±0.07	2.05
12	0(80)	0(20)	0(12.5)	2.09±0.08	2.01
13	0(80)	1(15)	-1(15)	2.74±0.06	2.82
14	1 (70)	0(20)	-1(15)	2.31±0.10	2.31
15	-1(90)	0(20)	1(10)	1.85±0.04	1.79
16	-1(90)	-1(25)	0(12.5)	2.71±0.03	2.82
17	0(80)	-1(25)	-1(15)	1.79±0.05	1.77

Table 3 ANOVA of the regression model for the prediction of emodin yield

Source	Sum of squares	df	Mean square	F value	p-Value
Model	2.66	9	0.30	25.57	0.0002**
X_1	0.011	1	0.011	0.91	0.3720
X_2	0.065	1	0.065	5.61	0.0498*
X_3	2.113×10^{-3}	1	2.113×10^{-3}	0.18	0.6818
X_1X_2	0.084	1	0.084	7.28	0.0308*
X_1X_3	0.011	1	0.011	0.95	0.3613
X_2X_3	0.13	1	0.13	11.21	0.0123*
X_1^2	0.89	1	0.89	77.00	0.0001**
X_2^2	0.60	1	0.60	51.85	0.0001**
X_3^2	0.62	1	0.62	53.93	0.0001**
Residual	0.081	7	0.012		
Lack of fit	0.045	3	0.015	1.64	0.3148
Pure error	0.036	4	9.070×10^{-3}		
Cor total	2.74	16			
C.V%		4.78			
R^2		0.9705			
Adj-R^2		0.9325			
Pre-R^2		0.8188			

Note : **: Highly significant coefficient (p<0.01)

*: Significant coefficient (p<0.05)

Table 4 The details interaction between emodin and LuxS protein

Donor Force	Receptor Force	Interaction Type
Emodin: OH	His14: N	Hydrogen bond
Emodin: OH	Glu60: O	Hydrogen bond
Emodin	Cys127	Hydrophobic
His61	Emodin	π-π stacking
Phe80	Emodin	π-π stacking

Figures

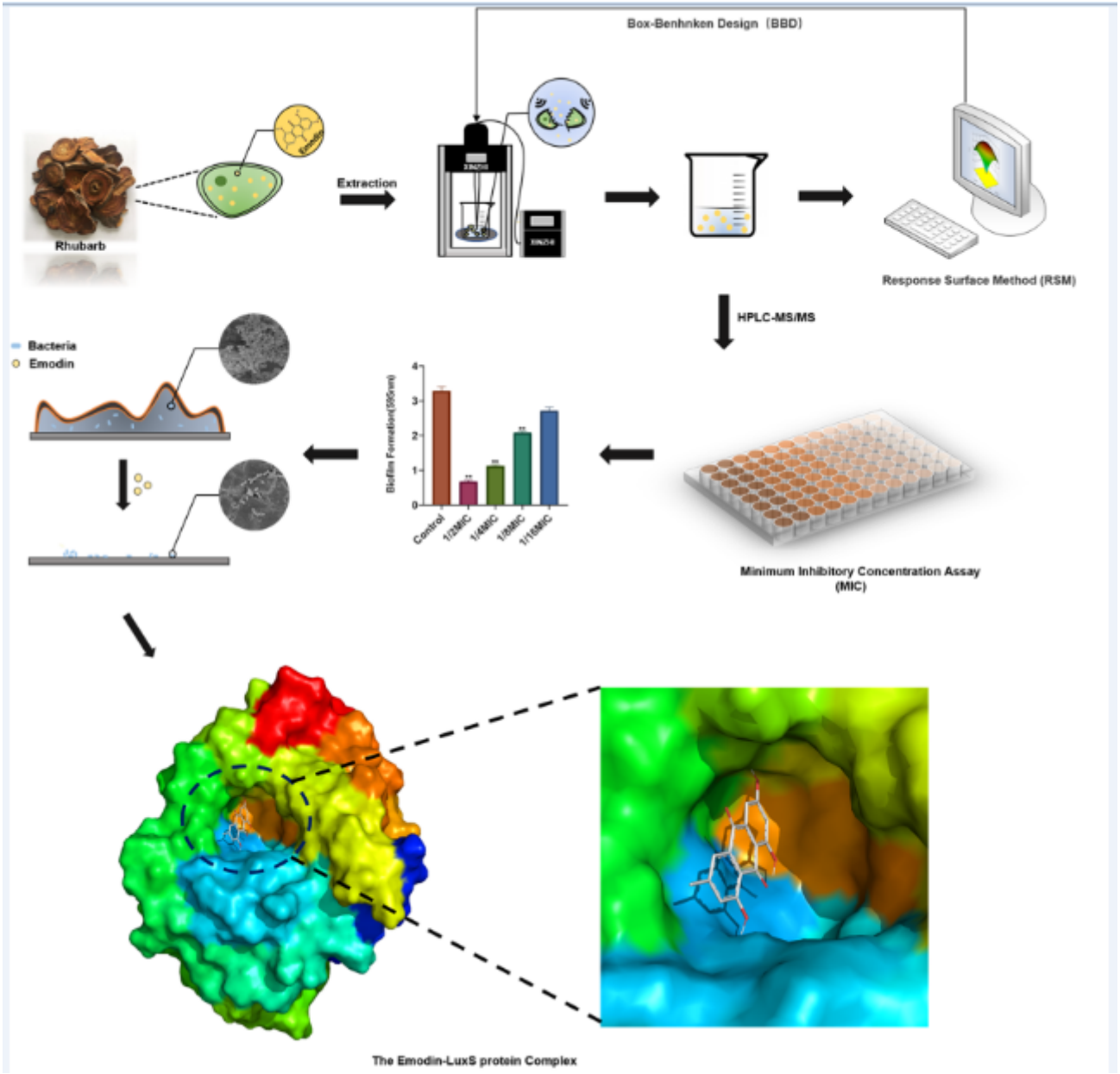

Figure 1

The graphic of specific experimental procedure.

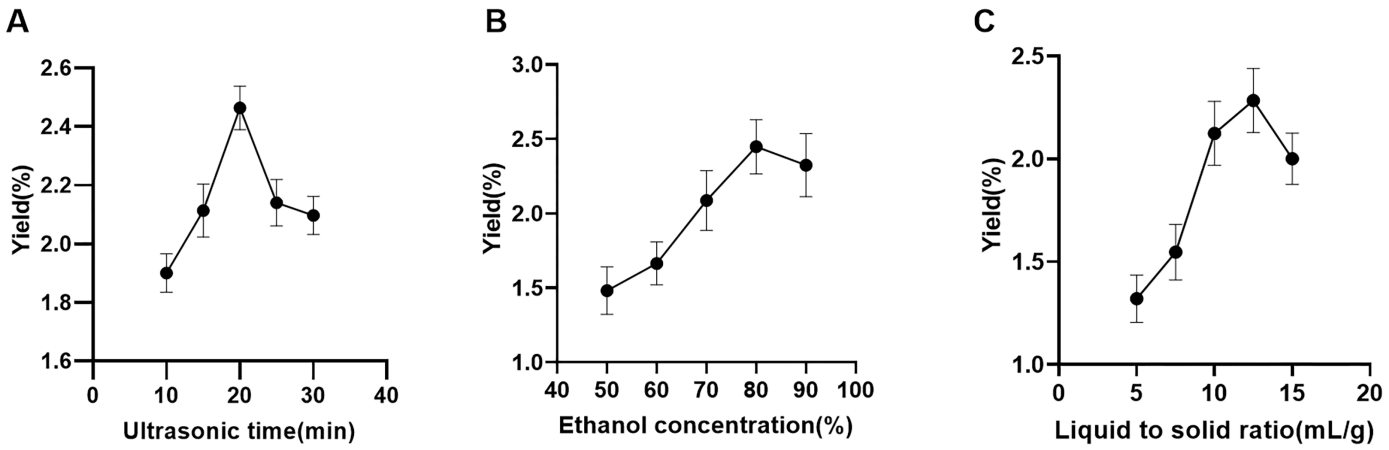

Figure 2

Single-factor experiments in emodin extraction from rhubarb. Three factors are considered such as ultrasonic time (A), ethanol concentration (B), and liquid to solid ratio (C). Data are representative of similar results obtained in 3 independent experiments.

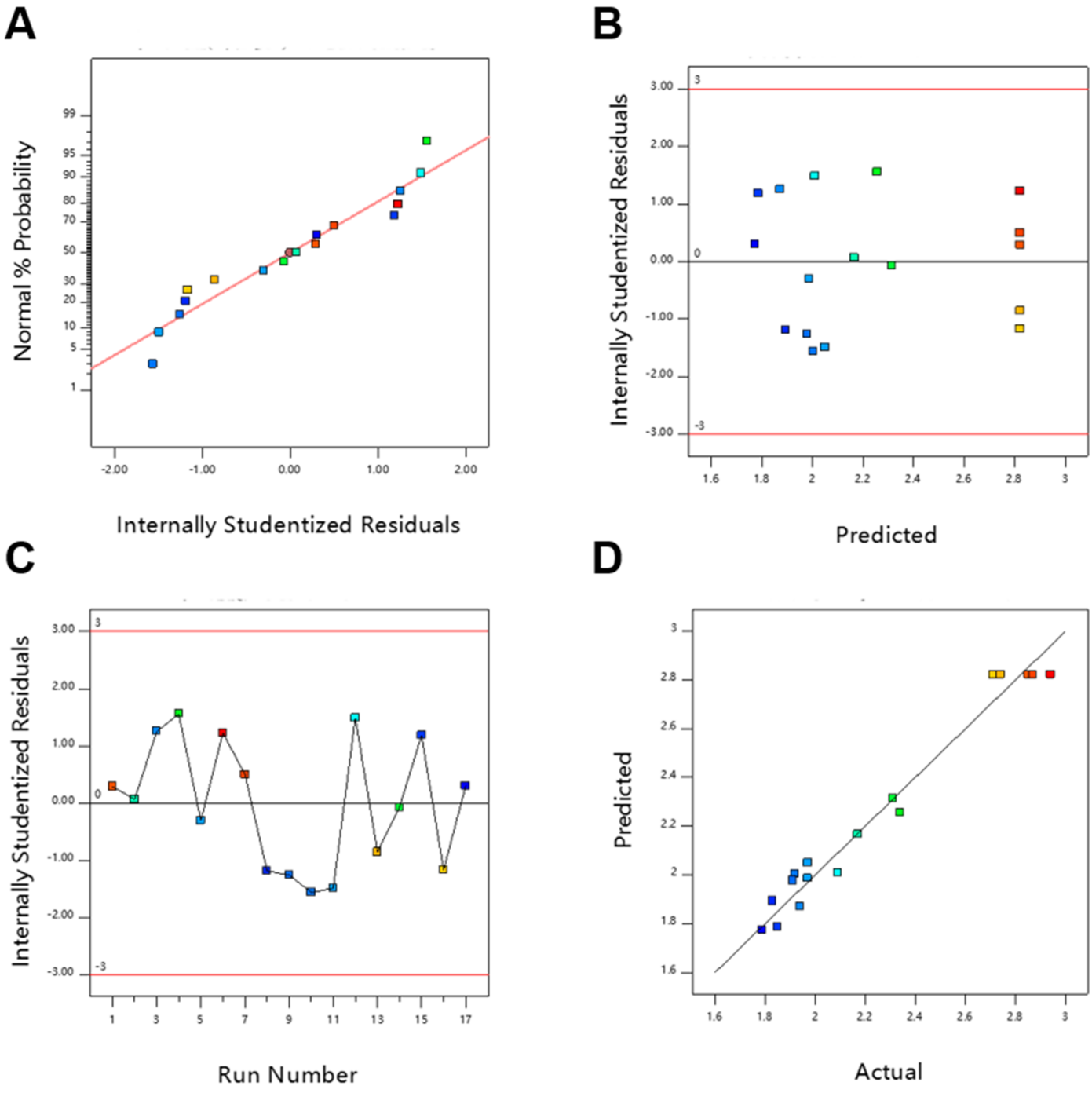

Figure 3

Diagnostic plots for the response surface model adequacy. (A) the normal % probability plot; (B) internally studentized residuals versus formula predicted;(C) internally studentized residuals versus experimental run; (D) predicted versus the actual values.

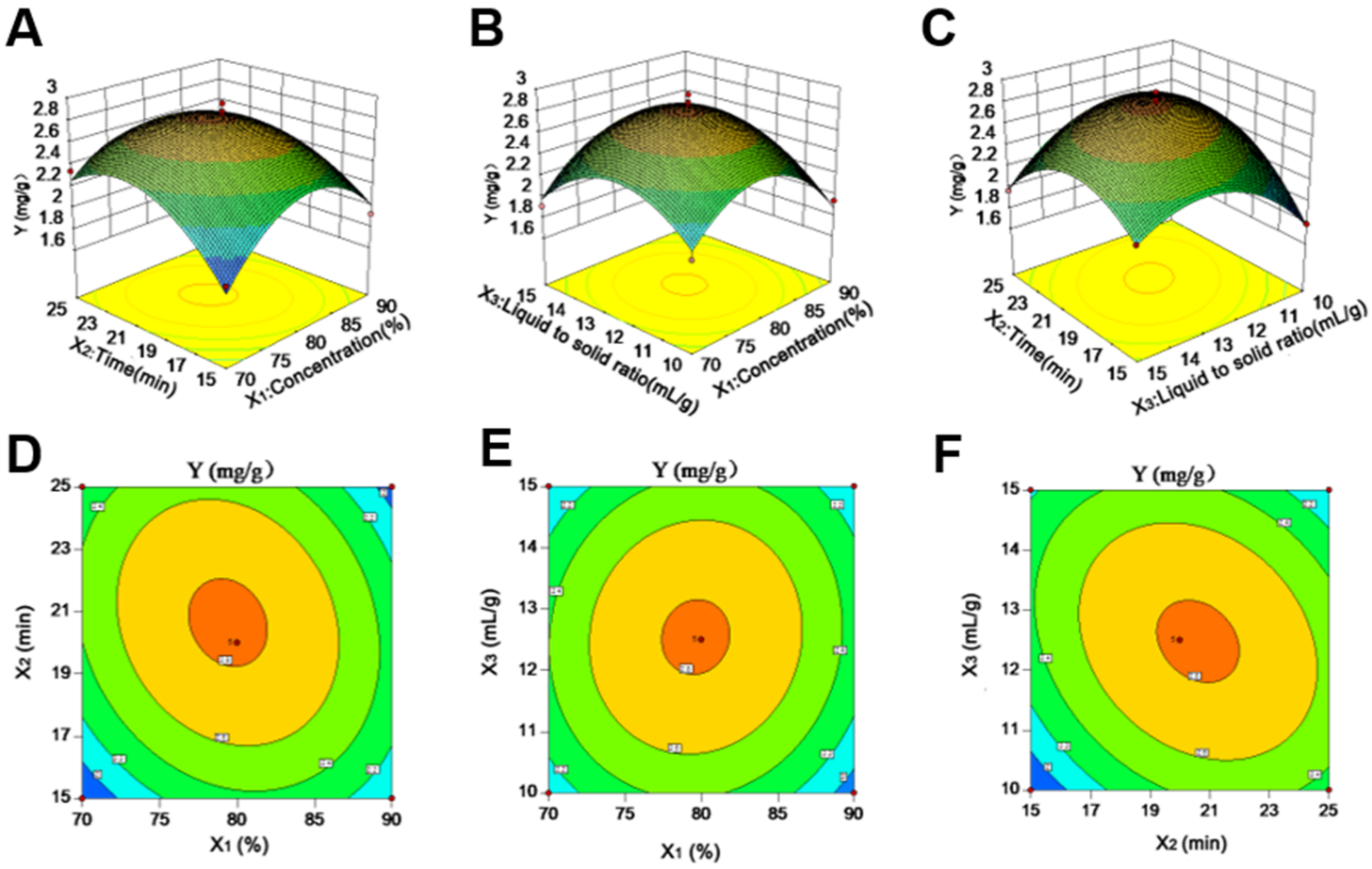

Figure 4

Response surface plots for the interaction effect (A) ethanol concentration vs extraction time; (B) ethanol concentration vs liquid to solid ratio; (C) extraction time vs liquid to solid ratio.

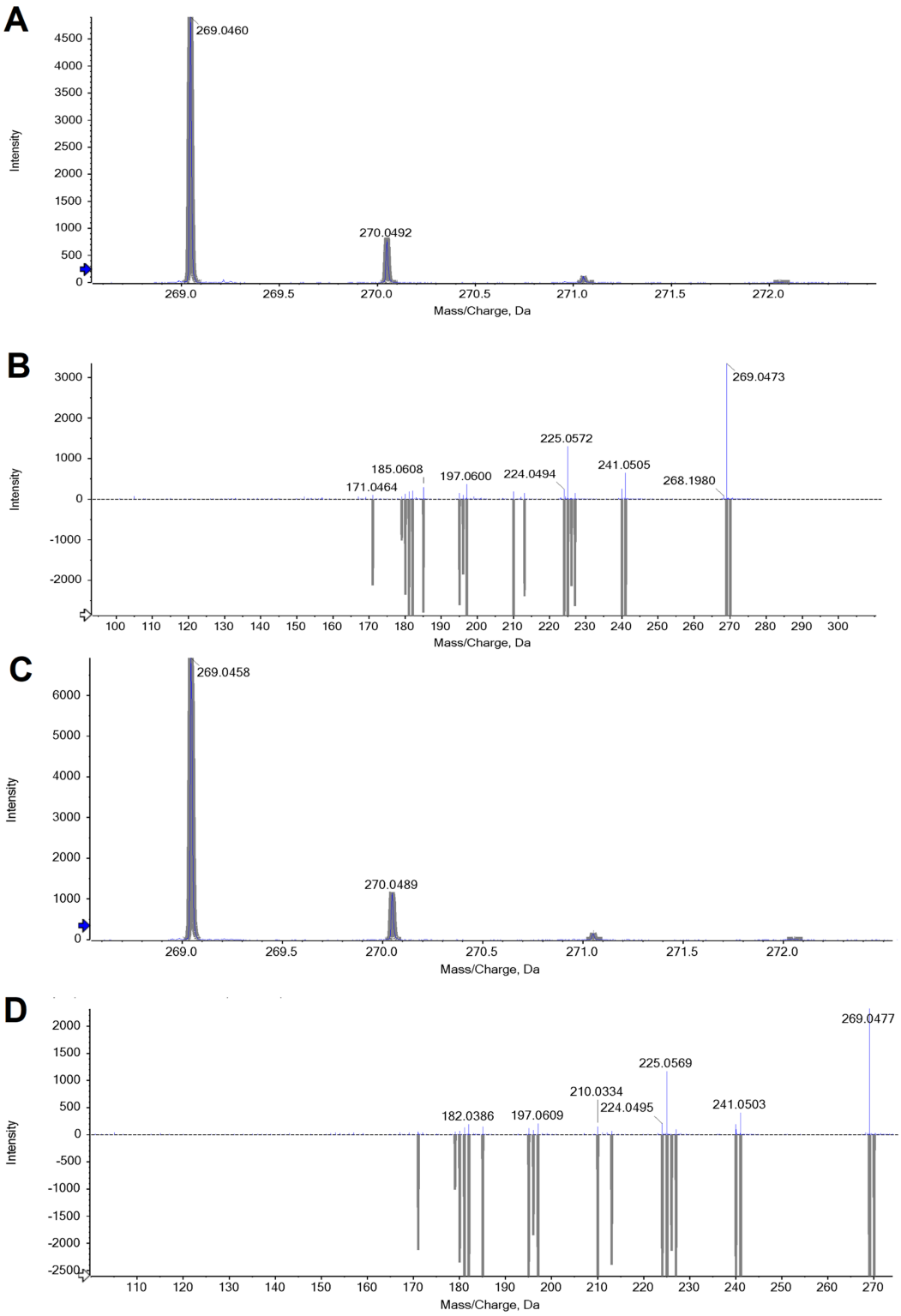

Figure 5

(A) presents the primary mass and (B) presents the secondary mass spectra of standard emodin; while (C) and (D) present the primary and secondary mass spectra of RUEP extracted from Rheum officinale Baill, respectively.

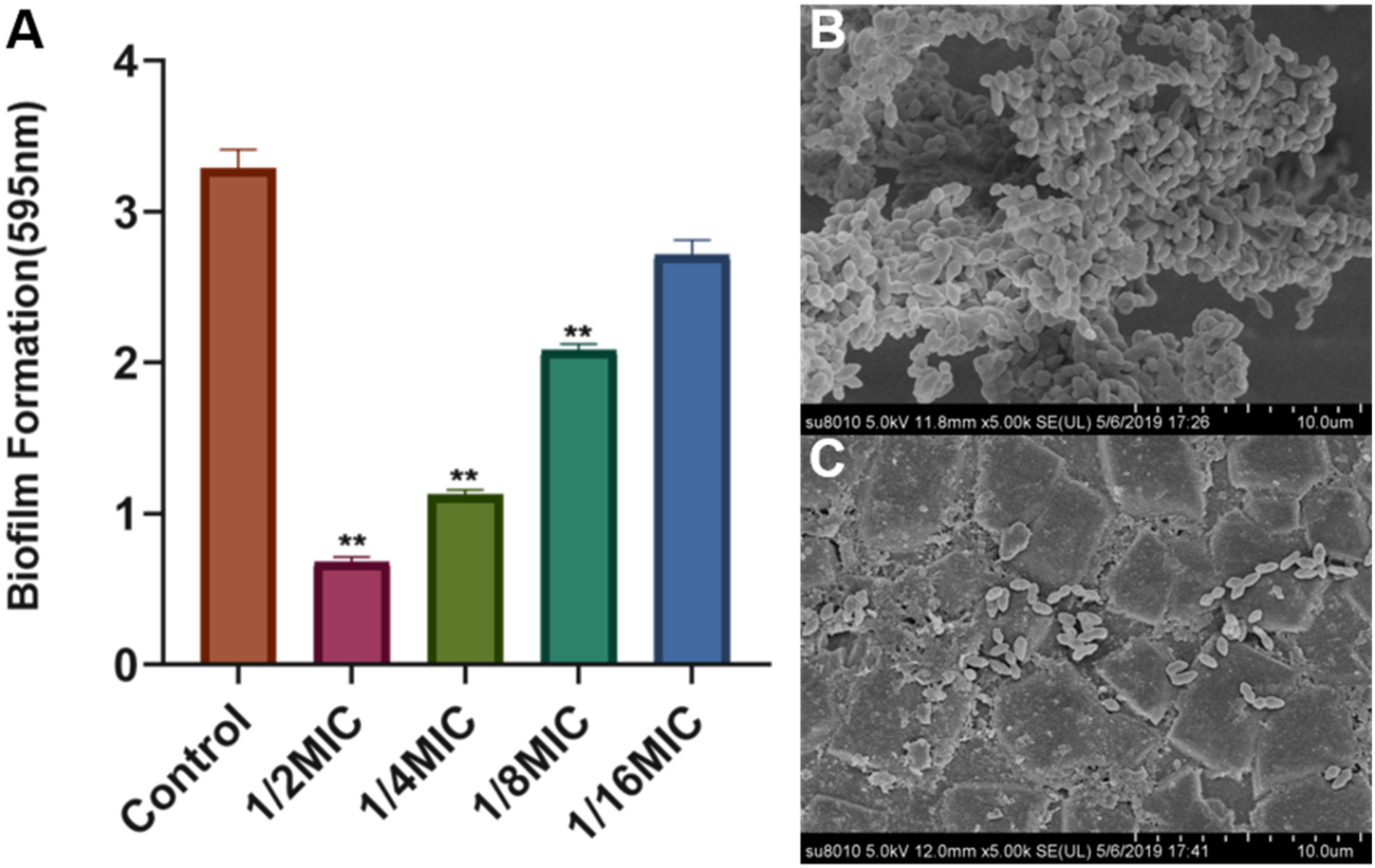

Figure 6

Effect of emodin on Streptococcus suis biofilm formation. The data were expressed as means ± SD (A). **p<0.01. Scanning electron micrographs of Staphylococcus suis biofilm formation in condition of no addition (B) or treated with 1/2 MIC of RUEP (C) in THB culture medium.

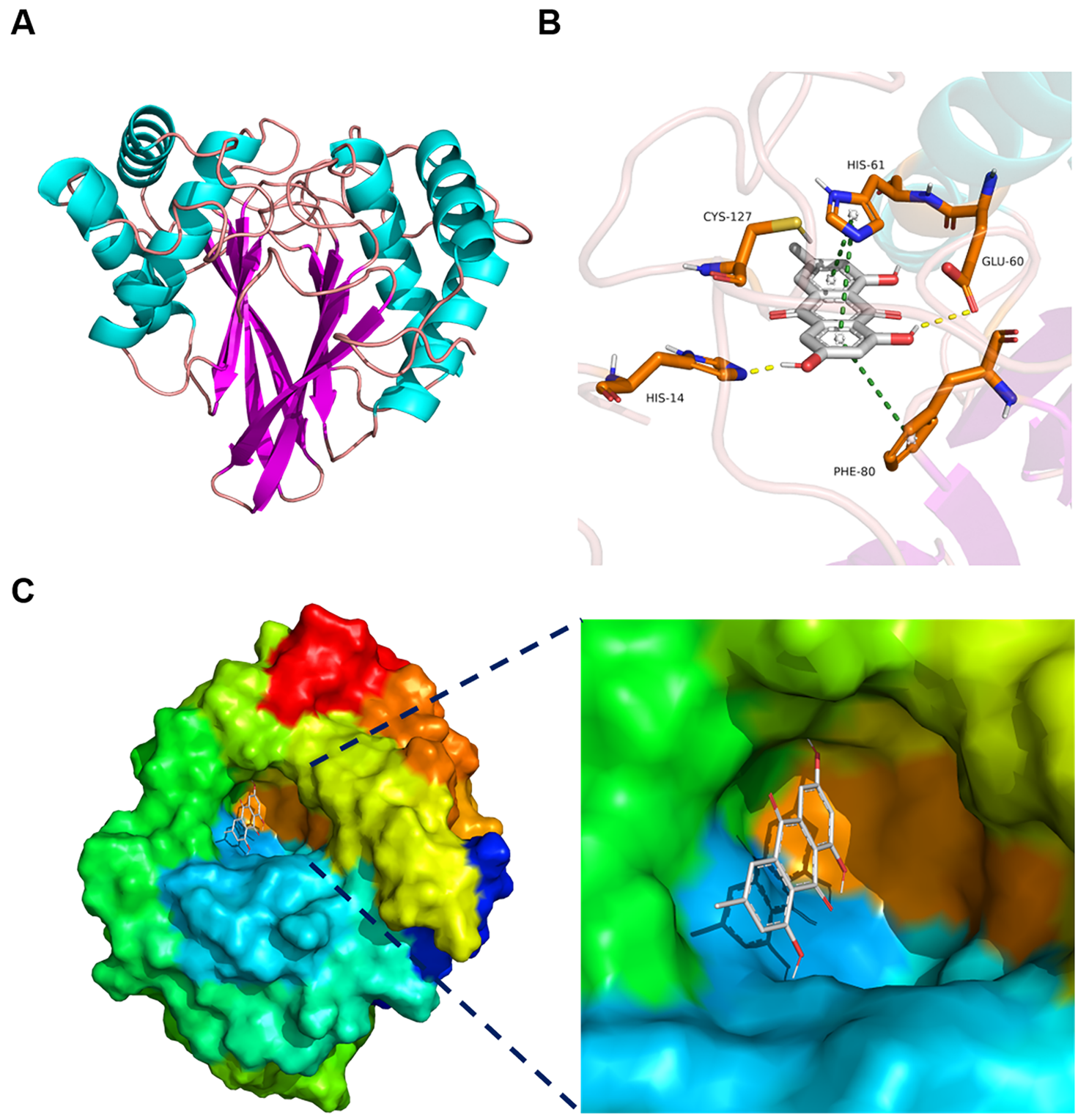

Figure 7

The complex structure model of emodin combine with the LuxS protein. (A) The structure of LuxS protein of S.suis. (B) Detailed binding mode of emodin. Emodin was presented as a white stick model. Amino acid residues were presented as an orange stick model. The yellow dashed lines indicated hydrogen bond and the green dashed lines indicated π-π stacking. (C) Overall view of emodin at cave-like active site.

Emodin was presented as a white line model. The LuxS protein was presented as a rainbow surface model.